Inhibition of Protein Phosphatase 2A Activity by Selective Electrophile Alkylation Damage†

Simona G. Codreanu,[‡,§] Deanna G. Adams,[||] Eric S. Dawson,[‡,⊥] Brian E. Wadzinski,*[,||] and Daniel C. Liebler*[,‡,§,||]

Departments of Biochemistry and Pharmacology, Mass Spectrometry Research Center, and Center for Structural Biology, Vanderbilt University School of Medicine, Nashville, Tennessee 37232

Received March 20, 2006; Revised Manuscript Received July 1, 2006

ABSTRACT: Protein serine/threonine phosphatase 2A (PP2A) is a critical regulator of numerous cellular signaling processes and a potential target for reactive electrophiles that dysregulate phosphorylation-dependent signal transduction cascades. The predominant cellular form of PP2A is a heterotrimeric holoenzyme consisting of a structural A, a variable B, and a catalytic C subunit. We studied the modification of two purified PP2A holoenzyme complexes ($AB\alpha_{FLAG}C$ and $AB\delta_{FLAG}C$) with two different thiol-reactive electrophiles, biotinyl-iodoacetamidyl-3,6-dioxaoctanediamine (PEO-IAB) and the biotinamido-4-[4′-(maleimidomethyl)cyclohexanecarboxamido]butane (BMCC). In vivo treatment of HEK 293 cells with these electrophiles resulted in alkylation of all three PP2A subunits. Electrophile treatment of the immunopurified FLAG-tagged holoenzymes produced a concentration-dependent adduction of PP2A subunits, as observed by Western blot analysis. Although both electrophiles labeled all three PP2A subunits, only BMCC inhibited the catalytic activity of both holoenzymes. Alkylation patterns in the A and B subunits were identical for the two electrophiles, but BMCC alkylated four Cys residues in the C subunit that were not labeled by PEO-IAB. Homology between the catalytic subunits of PP1 and PP2A enabled generation of a comparative model structure for the C subunit of PP2A. The model structure provided additional insight into contributions of specific BMCC−Cys adducts to PP2A enzyme inhibition. The results indicate that site selectivity of protein adduction should be a critical determinant of the ability of electrophiles to affect cellular signaling processes.

Reversible phosphorylation of proteins is one of the most crucial chemical reactions carried out by living organisms and plays a critical role in the regulation of cellular processes (*1*). This posttranslational modification alters properties of key regulatory proteins involved in specific pathways. Changes in the state of protein phosphorylation are regulated by protein kinases, which catalyze the formation of phosphate monoesters, and protein phosphatases, which reverse phosphorylation by hydrolysis (*2*). Recent evidence suggests that protein phosphorylation on either serine−threonine or tyrosine residues can be modulated by exogenously or intracellularly produced reactive oxygen species (*3*). Endogenously produced hydrogen peroxide, a mild oxidant that can oxidize cysteine residues in proteins, is a potent and reversible inhibitor of protein tyrosine phosphatases that affects tyrosine kinase signaling by inhibiting protein tyrosine dephosphorylation (*3*). Furthermore, reversible inhibitory modification of serine−threonine phosphatases by thiol−disulfide exchange and intermolecular disulfide formation demonstrated that protein phosphatases are oxidant-sensitive (*4*) and may serve as sensors for cellular stress responses.

The modification of serine−threonine phosphatases by oxidants and electrophiles takes on broad significance when considered in the context of oxidative stress and drug or chemical toxicity. Electrophilic products of xenobiotic metabolism and endogenous oxidative stress activate specific stress signaling networks (*5*−*7*). Although electrophiles may modify many proteins at once, some of these reactions may be particularly significant because they affect important control points for regulatory networks. The challenge in deciphering protein alkylation damage is in associating the selectivity of adduction with selectivity of effects. Thus, studies of specific proteins with significant roles in signaling offer a means of approaching this problem.

PP2A[1] is a major serine−threonine phosphatase that is expressed ubiquitously in eukaryotic cells, where it regulates a wide variety of cellular processes including translation, transcription, inflammation, differentiation, and apoptosis (*8*, *9*). The core enzyme is a dimer consisting of a 36 kDa catalytic C subunit tightly associated to a structural subunit A of a molecular mass of 65 kDa. This dimeric AC structure of PP2A forms a scaffold to which the appropriate regulatory B subunit can bind (*8*). The regulatory subunits play a key role in PP2A function by directing subcellular localization

† This work was supported by National Institutes of Health Grants ES011811 (D.C.L.), ES010056 (D.C.L.), ES000267 (D.C.L.), ES007028 (D.C.L.), GMO51366 (B.E.W.), and DK070787 (B.E.W.).

* To whom correspondence should be addressed. Phone: 615-322-3063. Fax: 615-343-8372. E-mail: daniel.liebler@vanderbilt.edu or brian.wadzinski@vanderbilt.edu.

‡ Department of Biochemistry, Vanderbilt University School of Medicine.

§ Mass Spectrometry Research Center, Vanderbilt University School of Medicine.

|| Department of Pharmacology, Vanderbilt University School of Medicine.

⊥ Center for Structural Biology, Vanderbilt University School of Medicine.

10.1021/bi060551n CCC: $33.50 © 2006 American Chemical Society
Published on Web 08/01/2006

and substrate selectivity. Within each serine−threonine phosphatase gene family, the catalytic domains are highly conserved, with functional diversity conferred by regulatory domains and subunits (*2*).

Protein subunits of the PP2A holoenzyme may be modified by electrophiles involved in cellular damage. Previous studies showed that chemical modification of sulfhydryl residues within the catalytic subunits of protein phosphatases 1 and 2A by thiol reactive reagents inactivated both enzymes (*10*). These two enzymes are structurally related, and their catalytic subunits share about 50% sequence identity (*8*). However, the mechanisms by which cellular thiol-reactive electrophiles inhibit the activity of the PP1 and PP2A enzymes, as well as the identities of target cysteine residue(s), remain unclear.

To probe the effects of electrophiles on PP2A enzymes, we employed two prototypical thiol-reactive electrophiles, PEO-IAB and BMCC, which represent thiol-modifying chemistries exhibited by a broad range of endogenous electrophiles and by environmentally and pharmacologically relevant agents (*5*, *6*, *11*, *12*). The iodoacetamide moiety in PEO-IAB reacts with thiols by an S_N2 mechanism involving displacement of the iodide leaving group by the thiol, whereas the maleimide moiety of BMCC is a Michael acceptor, in which thiols react with an α,β-unsaturated carbonyl system. We studied the modification of two purified FLAG-tagged PP2A holoenzymes ($AB\alpha_{FLAG}C$ and $AB\delta_{FLAG}C$) by these electrophiles. Although both electrophiles labeled all PP2A subunits for both holoenzymes, only the *N*-alkylmaleimide BMCC decreased PP2A catalytic activity. Adduct mapping by LC-MS-MS identified distinct modification patterns for the catalytic subunit of PP2A by the electrophiles. Differences in the adduction patterns provide insights into functionally critical residues and underscore the importance of site-specific reactions in determining the consequences of protein damage by electrophiles.

EXPERIMENTAL PROCEDURES

Materials. DMEM and fetal bovine serum were purchased from GIBCO (Rockville, MD). L-Glutamine, leupeptin, aprotinin, pepstatin, iodoacetamide, anti-FLAG M2 agarose, and anti-FLAG rabbit antibody were purchased from Sigma-Aldrich (St. Louis, MO). TCEP, IAB, PEO-IAB, and BMCC were from Pierce (Rockford, IL), and modified porcine sequencing grade trypsin was from Promega (Madison, WI). Penicillin, streptomycin, blasticidin, and hygromycin B were from Invitrogen (Carlsbad, CA). AlexaFluor680 conjugated fluorescent secondary antibodies were obtained from Molecular Probes (Eugene, OR), and IRDye800 conjugated fluorescent secondary antibodies were obtained from Rockland Immunochemicals (Gilbertsville, PA). Anti-biotin mouse monoclonal antibody was purchased from Roche (Indianapolis, IN), and PP2A catalytic subunit mouse monoclonal antibody was from BD Biosciences Pharmingen (San Diego, CA). Okadaic acid was from Calbiochem (San Diego, CA), and microcystin-LR was from Alexis Biochemicals (San Diego, CA). The generation and characterization of affinity-purified A- and Bα/δ-specific antibodies were as reported previously (*13*). All other chemical reagents were purchased from commercial sources and were used without further purification. All solutions were prepared fresh before each use.

In Vivo Treatment with Biotin-Linked Electrophiles. HEK 293 cells were grown in DMEM supplemented with 10% fetal bovine serum, 2 mM glutamine, 100 μg mL^{-1} penicillin, and 100 μg mL^{-1} streptomycin. Confluent cells plated in 150 mm dishes were washed with cold phosphate-buffered saline and incubated with 100 μM IAB, PEO-IAB, BMCC, or an equal volume of vehicle delivered in 10 mL of DMEM supplemented with 5% fetal bovine serum. Vehicle was dimethyl sulfoxide at 0.3% of total volume. Cells were exposed to electrophiles for 4 h at 37 °C in an atmosphere of 95% air/5% CO_2, then washed twice with ice-cold phosphate-buffered saline, and lysed in 1.5 mL of cold lysis buffer (50 mM Tris-HCl, 150 mM NaCl, 1 mM EDTA, 1 mM DTT, and 1% NP-40, pH 7.0, supplemented with protease inhibitor cocktail, 1.0 mM phenylmethanesulfonyl fluoride, 1.0 mM *N*-ethylmaleimide, 10 μg mL^{-1} leupeptin, 10 μg mL^{-1} aprotinin, and 10 μg mL^{-1} pepstatin) for each plate. The lysate was centrifuged at 10000*g* for 10 min to remove cellular debris, and the total protein concentration of the supernatant was determined by the BCA protein assay (Pierce).

Immunoblot Analysis of Electrophile-Treated HEK 293 Cells. To determine whether PP2A holoenzymes were alkylated by the biotinylated electrophiles in vivo, lysates from treated cells (prepared as described above) were incubated with streptavidin−agarose beads (~2 mg of protein per 1 mL^{-1} of bead slurry) for 1 h with rotation at room temperature. The bound proteins were washed three times with the above lysis buffer containing 1 M NaCl, twice with 0.1 M ammonium bicarbonate, pH 8.0, and once with deionized water. After each wash step, the beads were centrifuged at 10000*g* for 1 min, and the supernatant was discarded. The bound proteins were released from the beads by eluting the beads three times with 1 mL of 25% acetonitrile and 1.5 M formic acid for 20 min, while rotating the reaction tube at room temperature. The eluted fractions were pooled together and concentrated to 100 μL using 10000 molecular weight cutoff Amicon Ultra concentrators (Millipore, Bedford, MA), and the buffer was exchanged using the concentrator with 2 mL of 0.1 M ammonium bicarbonate, pH 8.0. Aliquots of the protein eluates (25 μL) then were subjected to immunoblot analyses.

Both crude cellular lysate from treated cells and adducted proteins purified by streptavidin capture as described above were resolved by 10% SDS−PAGE using NuPAGE Bis-Tris gels (Invitrogen). The proteins were electrophoretically transferred to a nitrocellulose membrane (Invitrogen) and probed with antibodies for A, Bα/δ, and C subunits or mouse anti-biotin. AlexaFluor680-labeled goat anti-rabbit secondary antibody was used to detect A and Bα/δ subunits, and AlexaFluor680-labeled goat anti-mouse antibody was used to detect C subunit and biotinylated proteins. Immunoreactive

[1] Abbreviations: $AB\alpha_{FLAG}C$, protein phosphatase 2A holoenzyme containing A subunit, FLAG-tagged Bα subunit, and C subunit; $AB\delta_{FLAG}C$, protein phosphatase 2A holoenzyme containing A subunit, FLAG-tagged Bδ subunit, and C subunit; BMCC, biotinamido-4-[4′-(maleimidomethyl)cyclohexanecarboxamido]butane; DiFMUP, 6,8-difluoro-4-methylumbelliferyl phosphate; DMEM, Dulbecco's modified Eagle's medium; DTT, dithiothreitol; ER, endoplasmic reticulum; IAB, *N*-iodoacetyl-*N*-biotinylhexylenediamine; LC-MS-MS, liquid chromatography−tandem mass spectrometry; MS-MS, tandem mass spectrometry; PEO-IAB, biotinyl-iodoacetamidyl-3,6-dioxaoctanediamine; PP1, protein phosphatase 1; PP2A, protein phosphatase 2A; TCEP, tris-(2-carboxyethyl)phosphine.

proteins were visualized using the Odyssey infrared imaging system and Odyssey software as described by the manufacturer (Li-Cor, Lincoln, NE).

Expression and Purification of PP2A ABα_{FLAG}C or ABδ_{FLAG}C Holoenzymes. Both FLAG-tagged Bα- or Bδ-containing PP2A holoenzymes were purified from HEK T-Rex cells as previously described (*13*, *14*). Briefly, cell lines stably expressing plasmids encoding FLAG-tagged B subunits ($B\alpha_{FLAG}$ and $B\delta_{FLAG}$) in a tetracycline-inducible system were maintained in DMEM supplemented with 10% FBS, 5 μg mL^{-1} blasticidin, and 175 μg mL^{-1} hygromycin B. Cell extracts were prepared 48 h post-tetracycline induction of protein expression. A stable HEK T-Rex cell line expressing the empty vector was used as control. FLAG-tagged proteins were immunopurified using anti-FLAG M2 agarose and eluted from the beads with the FLAG peptide. Aliquots of the purified holoenzymes were resolved by 10% SDS−PAGE and analyzed by immunoblotting with specific antibodies recognizing the FLAG epitope and PP2A subunits (A, Bα/*δ*, or C).

Immunoblot Analysis of in Vitro Electrophile Treatment of PP2A Holoenzymes. Equal amounts of FLAG eluates of immunoprecipitation from an empty vector, $B\alpha_{FLAG}$, or $B\delta_{FLAG}$ expressing cells were incubated with increased concentrations of electrophile for 30 min at 37 °C to generate protein adducts. Due to their different reactivity toward proteins, the electrophiles were used over a different concentration range, with PEO-IAB varying between 0 and 100 μM and BMCC varying between 0 and 25 μM. The adduct formation reaction was quenched by the addition of DTT to a final concentration of 5 mM. Adduct formation was characterized by immunoblotting with an anti-biotin mouse monoclonal antibody.

Protein Phosphatase Activity Measurements of Electrophile-Treated PP2A Holoenzymes. Radiolabeled PKA-phosphorylated histone H1 was prepared as described previously (*15*, *16*). Electrophile-treated PP2A holoenzymes (∼9 ng) were assayed for phosphatase activity in a 50 μL reaction mixture containing phosphatase assay buffer and ^{32}P-labeled histone H1 (*14*). After 15 min incubation at 30 °C, the reactions were terminated by the addition of trichloroacetic acid to a final concentration of 20%. The samples were incubated on ice for 30 min, and proteins were pelleted by centrifugation at 13000*g* for 10 min. Supernatants were collected and quantified for [^{32}P]P_i release by liquid scintillation counting. Less than 20% of total phosphorylated substrate was dephosphorylated during the assays, thus ensuring that substrate was not limiting. Statistical analysis was performed using GraphPad Prism 4 (GraphPad Software, San Diego, CA).

For phosphatase assays using DiFMUP as a substrate, electrophile-treated ABα_{FLAG}C or ABδ_{FLAG}C holoenzymes were diluted with phosphatase assay buffer (50 mM Tris-HCl, pH 7.0, 0.1 mM $CaCl_2$, and 3.2 mg mL^{-1} bovine serum albumin) to a final volume of 80 μL. Phosphatase assays were performed in a 96-well microplate using a FLEXstation (Molecular Devices, Sunnyvale, CA) with Softmax Pro 4.3.1 DD software (Molecular Devices). The fluorogenic substrate, DiFMUP (Molecular Probes, Eugene, OR) was diluted in 50 mM Tris-HCl, pH 7.0, and added by the FLEXstation arm in a volume of 120 μL to each well (for a final concentration of 100 μM); the final volume for each reaction was 200 μL. All the assays were carried out at 37 °C for 10 min. Fluorescence of the DiFMUP hydrolysis product was measured at 10 s intervals using excitation and emission wavelengths of 358 and 455 nm, respectively. Background fluorescence (FLAG eluates of immunoprecipitation from empty vector cells) was subtracted from the raw data. Statistical analysis was performed using GraphPad Prism 4 (GraphPad Software, San Diego, CA).

Competition Analysis. For competition experiments, purified PP2A holoenzymes were pretreated with 1 μM microcystin or 1 μM okadaic acid (concentrations that are known to inhibit PP2A holoenzymes) for 30 min at 37 °C. Subsequently, samples were incubated with BMCC for 30 min at 37 °C at a final concentration of 25 μM. The adduct formation reaction was quenched by the addition of DTT to a final concentration of 5 mM. The reaction mixture was characterized by immunoblotting with anti-biotin mouse monoclonal antibody, and the modifications were analyzed by LC-MS-MS.

In-Gel Digestion of Adducted Proteins. Equal amounts (∼500 μL) of FLAG eluates of immunoprecipitation from an empty vector, $B\alpha_{FLAG}$, or $B\delta_{FLAG}$ expressing cells were incubated with either 25 μM BMCC or 100 μM PEO-IAB for 30 min at 37 °C to generate protein adducts. The adduct formation reaction was quenched by the addition of DTT to a final concentration of 5 mM, and the reaction mixture was concentrated to 50 μL using 10000 molecular weight cutoff Amicon Microcon filters (Millipore). Unreacted DTT and BMCC were washed out by buffer exchange with 0.1 M ammonium bicarbonate, pH 8.0, using the same technique. Adducted proteins were resolved by 10% SDS−PAGE using NuPAGE Bis-Tris gels and stained with colloidal Coomassie blue (Invitrogen). Bands corresponding to individual subunits were excised from the gel and digested in-gel with trypsin (*17*).

LC-MS-MS Analyses. LC-MS-MS analyses were performed with a Thermo LTQ instrument (Thermo Electron, San Jose, CA) equipped with a Thermo Surveyor solvent delivery system, autosampler, and a microelectrospray source. Peptides were resolved on a 100 μm × 11 cm fused silica capillary column (Polymicro Technologies, LLC, Phoenix, AZ) packed with 5 μm, 300 Å Jupiter C18 (Phenomenex, Torrance, CA). Liquid chromatography was carried out at ambient temperature at a flow rate of 0.6 μL min^{-1} using a gradient mixture of 0.1% (v/v) formic acid in water (solvent A) and 0.1% (v/v) formic acid in acetonitrile (solvent B). Peptides eluting from the capillary tip were introduced into the LTQ source with a capillary voltage of approximately 2.4 kV. The heated capillary was operated at 150 °C and 40 V. MS-MS spectra were acquired in the data-dependent scanning mode consisting of a full scan obtained for eluting peptides in the range of 350−2000 amu followed by four data-dependent MS-MS scans. MS-MS spectra were recorded using dynamic exclusion of previously analyzed precursors for 30 s with a repeat duration of 2 min. MS-MS data were analyzed using the SEQUEST algorithm (*18*) to evaluate protein coverage and to identify spectra of protein adducts. Mass shifts of +533, +414, and +430 corresponding to BMCC, PEO-IAB, and oxidized PEO-IAB were used as variable modifications to identify spectra of adducts. The P-Mod program was also used to identify MS-MS spectra corresponding to alkylated PP2A peptide sequences (*19*). All

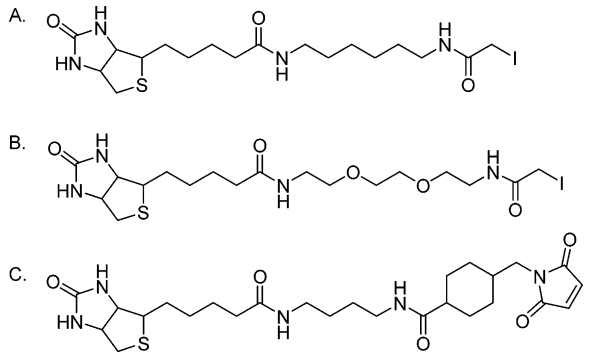

FIGURE 1: Chemical structures of IAB (A), PEO-IAB (B), and BMCC (C).

adducts were characterized by mass shifts of the b- and y-series ions that confirmed sequence localization.

Molecular Modeling and Visualization. To visualize sites of BMCC adduction within the PP2A catalytic subunit protein structure, a preliminary molecular model of the PP2A catalytic domain was constructed using chain A from the crystal structure of the catalytic subunit of the PP1 δ protein isoform (PDB ID 1S70) that featured two copies of the protein in the crystallographic unit cell. EsyPred3D, a new automated homology modeling webserver (*20*), was utilized to obtain the initial model. The EsyPred3D alignment algorithm makes use of consensus multisequence alignments that are combined, weighted, and screened using artificial neural network pattern recognition algorithms. This approach produced enhanced sequence alignments and identified the PP1 δ protein isoform (Figure S10, Supporting Information) as the best template structure for modeling the catalytic subunit of PP2A. The model-building algorithm in this program makes use of the comparative modeling software package Modeller to construct the coordinates of the PP2A protein. The resulting initial model for PP2A was aligned to the protein backbone structure of microcystin-adducted PP1 (PDB ID 1FJM) to obtain positions for coordinated Mn^{2+} ions in the PP2A catalytic subunit active site (Figure S11, Supporting Information). Preliminary model building combined with visual inspection aided our positioning of the BMCC-adducted cysteine residues identified in this study relative to important catalytic residues in the PP2A enzyme active site. The UCSF Chimera software package was used for all molecular visualization and generation of Figures 7, 8, and S11 (Supporting Information) (*21*).

RESULTS

Reactive Electrophiles Alkylate PP2A in Intact Cells. To investigate the effects of covalent adduction on the enzymatic activity of PP2A and to evaluate the mechanism of inhibition of this enzyme, we employed three thiol-reactive electrophiles, IAB, PEO-IAB, and BMCC, which display two distinct reactive chemistries (Figure 1). We have used these probes in other recent studies and have shown that they penetrate cells, bind covalently to proteins, and activate specific stress responses (*11*). We also have defined the characteristics of covalent thiol adduction by these probes on a proteomic scale (*12*).

To determine whether PP2A subunits are alkylated by electrophiles in vivo, both crude cellular lysate from treated cells and adducted proteins purified by streptavidin capture

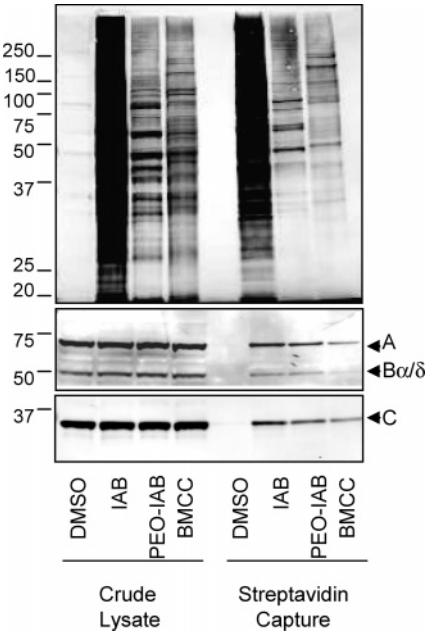

FIGURE 2: In vivo identification of the PP2A holoenzyme as a target of alkylation-induced cellular stress. HEK 293 cells were incubated with 100 μM IAB, PEO-IAB, BMCC, or vehicle (DMSO) for 4 h at 37 °C. After cell lysis, the biotinylated proteins were precipitated using immobilized streptavidin. An aliquot of the treated lysates and streptavidin-captured proteins was resolved by SDS−PAGE, transferred to nitrocellulose membranes, and immunoblotted with an anti-biotin antibody (upper panel) or antibodies recognizing A, Bα/δ, or C subunits (lower panels).

were analyzed by immunoblotting with anti-biotin mouse monoclonal antibody (Figure 2). Detection of the biotin-adducted proteins in the streptavidin-purified samples by the anti-biotin antibody demonstrated that all three thiol-reactive electrophiles covalently bind to cellular proteins and that adducts are stable in the presence of denaturants. We also noticed that each compound exhibited a different pattern of adduction, which suggested that different adduction chemistries can affect specificity for cellular targets. These observations are consistent with other recent studies (*21*). The greatest degree of adduction was observed with IAB, which is the smallest and most lipid soluble probe. Immunoblot analysis of streptavidin-captured proteins from treated cells with antibodies specific for individual A, Bα/δ, or C subunits of PP2A indicated that all three were adducted by the electrophiles.

In Vitro Treatment of PP2A ABα_{FLAG}C or ABδ_{FLAG}C Holoenzymes with BMCC Decreases Protein Phosphate Activity. Since there are many phosphatases present in the intact cell and no assay to easily distinguish among them, we could not directly evaluate the effects of alkylation on PP2A enzymatic activity in vivo. To investigate the sites of adduction by different electrophiles and the effects on enzymatic activity of adducted species, two PP2A holoenzymes (ABα_{FLAG}C or ABδ_{FLAG}C) were incubated in vitro with increasing concentrations of electrophiles. Due to their different reactivities toward the proteins, the electrophiles were used over different concentration ranges, with PEO-IAB varying between 0 and 100 μM and BMCC varying between 0 and 25 μM. Electrophile concentrations were maintained as low as possible for detection of adducts, yet were still those producing nonlethal signaling perturbations

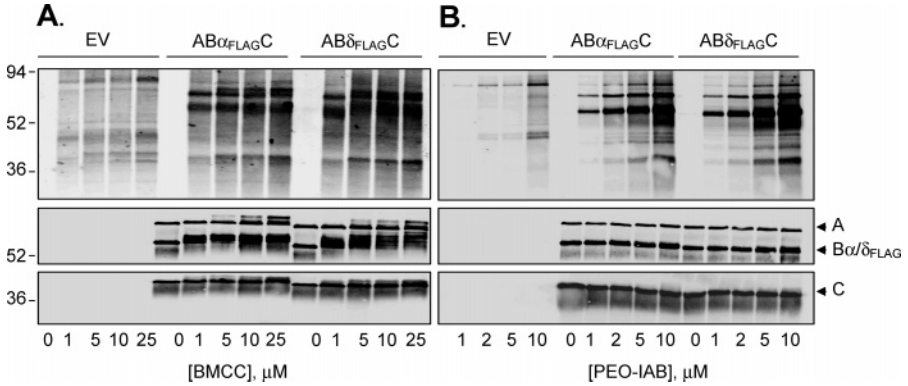

FIGURE 3: In vitro electrophile treatment produced a dose-dependent increase in adduct formation of PP2A subunits. Equal amounts of FLAG peptide eluates from FLAG immune complexes of cells expressing empty vector (EV), Bα_{FLAG}, or Bδ_{FLAG} were incubated for 30 min at 37 °C with increasing concentrations of BMCC (panel A) or PEO-IAB (panel B) for 30 min. The adduct formation reaction was quenched by adding DTT. Reaction mixtures were resolved by SDS−PAGE, and adduction of PP2A subunits was determined by immunoblotting with a mouse anti-biotin monoclonal antibody (top panels). PP2A subunits were visualized by immunoblotting with antibodies recognizing the A, Bα/δ_{FLAG}, or C subunits (bottom panels).

in intact cells (*11*). As shown in Figure 3, Western blotting with the anti-biotin antibody revealed that in vitro treatment with both electrophiles, BMCC (panel A) and PEO-IAB (panel B), produced a dose-dependent increase in adduct formation for each individual subunit and that both probes labeled all three subunits. Although the degree of adduction by the two electrophiles was similar, adduction by BMCC, but not by PEO-IAB, caused concentration-dependent perturbations in electrophoretic migration of the A and B subunits (see the middle panels in Figure 3). Immunoblots with antibodies to the A and B subunits indicate that the BMCC-adducted A and B subunits migrate differently than the unadducted proteins. This effect is not evident in the upper panel of Figure 3A, which only shows biotinylated (adducted) proteins. The different effects of the electrophiles on migration are apparently not due to differences in alkylation site selectivity (see below) but may reflect different effects of the adducts themselves on protein folding or SDS binding. This interesting effect was not further investigated in this study.

We next examined the ability of these reactive electrophiles to inhibit the phosphatase activity of PP2A. We first utilized the protein substrate ^{32}P-labeled histone H1. Although both electrophiles labeled all PP2A subunits, only BMCC caused a significant decrease (~75%) in the catalytic activity for both holoenzymes (Figure S1, Supporting Information). The inhibition could reflect effects on substrate binding, catalysis, or both. Electrophile binding to reactive cysteine residues may interfere with binding of the relatively large histone substrate and block presentation of the phosphorylated residue to the active site for the dephosphorylation reaction. Thus, we also assayed phosphatase activity using the small molecule substrate DiFMUP (Figure 4). Consistent with the histone H1 assays, there was a significant decrease in DiFMUP phosphatase activity for the BMCC-adducted holoenzymes, whereas no inhibition was produced by PEO-IAB.

Identification of Electrophile Adduction Sites on PP2A ABα_{FLAG}C or ABδ_{FLAG}C Holoenzymes. To identify the sites of electrophile adduction on PP2A holoenzymes, we used LC-MS-MS analyses. Equal amounts of ABα_{FLAG}C or ABδ_{FLAG}C were incubated with 25 μM BMCC or 100 μM PEO-IAB for 30 min at 37 °C. These concentrations of electrophiles produced approximately equal levels of adduct formation as determined by immunoblot analyses (Figure 3). Reactions were quenched with DTT and concentrated with spin filters, and the PP2A subunits were resolved by SDS−PAGE (Figure S3, Supporting Information). Bands containing individual subunits were excised from the gel and subjected to in-gel tryptic digestion. The peptide mixtures were analyzed by LC-MS-MS, and adduction sites were identified by analyzing the data with the Sequest and P-Mod algorithms. Data from three independent experiments are summarized in Table 1 and Table 2 (Supporting Information), where empty cells indicate that the corresponding peptide was detected only as the *S*-carboxamidomethyl derivative formed by reduction and alkylation of unmodified cysteine thiols with iodoacetamide during sample preparation. Electrophile-adducted cysteines are indicated as the number of times the adducted peptide was detected from the total number of replicate experiments. Certain cysteine-containing peptides were not detected (ND) in either *S*-carboxamidomethyl or electrophile-adducted forms, which indicated that these peptides either were not generated efficiently by tryptic digestion, displayed poor chromatographic properties, or ionized poorly in electrospray, thus making them difficult to detect.

For the structural subunit A, LC-MS-MS analyses generated MS-MS spectra corresponding to approximately 80% of the protein sequence. In both the ABαC or ABδC holoenzymes, eight peptides were adducted by PEO-IAB, accounting for 10 cysteine residues out of 14 present in the A subunit. Six peptides containing seven A subunit cysteines were adducted by BMCC. The conformation of the A subunit is defined by 15 tandemly repeated HEAT sequence motifs, each consisting of a pair of antiparallel α helices that assemble to form an elongated structure characterized by a double layer of α helices (*22*). All adducted cysteine residues in the A subunit were either within the flexible loops that connect the helices or faced the intramolecular space between the structural motifs. These spaces allow for high solvent accessibility and can be easily targeted by reactive electrophilic species.

LC-MS-MS analyses of the regulatory subunit B generated MS-MS spectra corresponding to approximately 80% of the protein sequence. Four peptides adducted by both PEO-IAB

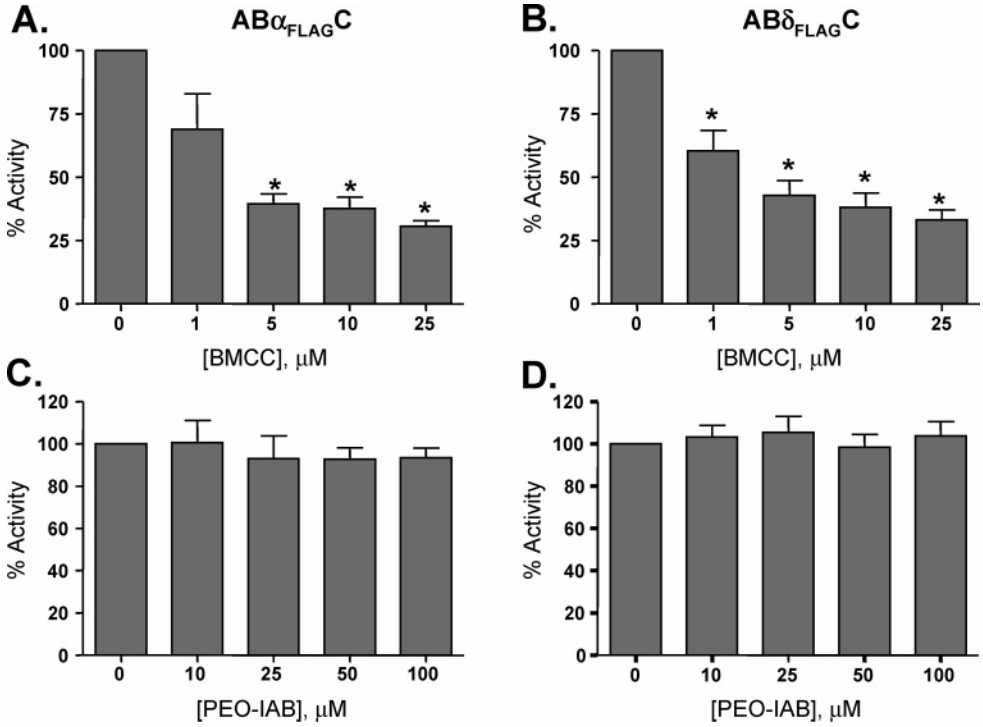

FIGURE 4: Electrophile treatment produced a dose-dependent decrease in PP2A catalytic activity. The purified PP2A holoenzymes, ABα$_{FLAG}$C and ABδ$_{FLAG}$C, were pretreated with increasing concentrations of BMCC (A and B) or PEO-IAB (C and D) and then assayed for activity using the fluorogenic DiFMUP substrate. Phosphatase activities (10 min incubation) of the treated samples are expressed as a percent of the activities of vehicle-treated samples, which are set at 100%. Shown are the mean ± SD for three independent experiments. Phosphatase activity was significantly different in ABα$_{FLAG}$C or ABδ$_{FLAG}$C holoenzyme preparations treated with BMCC as compared to vehicle-treated samples when analyzed by Student's *t*-test: *, $p < 0.05$.

Table 1: Sites of BMCC and PEO-IAB Modification of the Catalytic Subunit of PP2A Holoenzymes[a]

peptide sequence[b]	Cys no.	ABαC PEO-IAB	ABαC BMCC	ABδC PEO-IAB	ABδC BMCC
ELDQWIEQLNE**C***K	C20		**3/3**[c]		**3/3**
SL**C***EK	C32				
C*P̄VTV**C***GDVHGQFHDLMELFR	C50−C55	ND[d]	ND	ND	ND
Q̄ITQVYḠFYDE**C***LR	C133		**2/3**		**2/3**
YFTDLFDYLPLT̄ALVDGQIF**C***LHGGLSPSIDTLDHIR	C165	ND	ND	ND	ND
LQEVPHEGPM**C***DLLWSDPD̄DR	C196				**2/3**
AHQLVMEGYN̄W**C***HDR	C251		**2/3**		**2/3**
NVVTIFSAPNY**C***ȲR	C266	2/3	3/3	3/3	3/3
C*GNQAAIMEL̄DDTLK	C269	3/3	3/3	2/3	3/3

[a] Equal amounts of ABα$_{FLAG}$C or ABδ$_{FLAG}$C holoenzyme were incubated with 25 μM BMCC or 100 μM PEO-IAB for 30 min at 37 °C and then quenched by DTT, concentrated by spin filters, and resolved by SDS−PAGE. Individual subunits were cut from the gel, followed by in-gel trypsin digest, and the peptides were analyzed by LC-MS-MS. [b] The asterisk indicates adducted cysteine residues. [c] Indicates the number of times an adducted peptide was detected/number of experiments. Cys residues adducted by BMCC only are underlined and in bold type. [d] ND indicates peptides not detected as either S-carboxamidomethylated or adducted. Empty cells indicate that the corresponding peptide was detected as an *S*-carboxamidomethyl derivative as a result of reduction and alkylation with iodoacetamide.

and BMCC contained four of nine possible cysteine residues in the Bα isoform and 10 possible cysteine residues for Bδ. The same pattern of B subunit adduction was observed for both enzyme isoforms with either PEO-IAB or BMCC treatment. The regulatory B subunit binds and interacts via the same or overlapping sites with the A subunit of the core dimer and serves to localize the phosphatase to specific subcellular locations (*8*). The structures of the B subunits have not been reported.

LC-MS-MS analyses of the catalytic subunit C generated MS-MS spectra corresponding to approximately 70% of the protein sequence and showed a different pattern of adduction for the two compounds. Only two peptides containing two cysteine residues out of 10 total were adducted by PEO-IAB. In contrast, BMCC adducted six peptides containing six cysteines, which included Cys 20, Cys 133, Cys 196, Cys 251, Cys 266, and Cys 269. The only two cysteine residues adducted by both BMCC and PEO-IAB were Cys 266 and Cys 296. Cys 196 adduction was only observed upon BMCC treatment of the Bδ isoform. Together with the LC-MS-MS analyses of the A and B subunits which showed a similar number of peptides labeled with both compounds, these results suggest that certain BMCC adducts on the catalytic subunit are responsible for the decrease in enzymatic activity of the PP2A holoenzymes. MS-MS spectra of all peptides from the PP2A catalytic subunit adducted with either BMCC or PEO-IAB are presented as Supporting Information (Figures S4−S9).

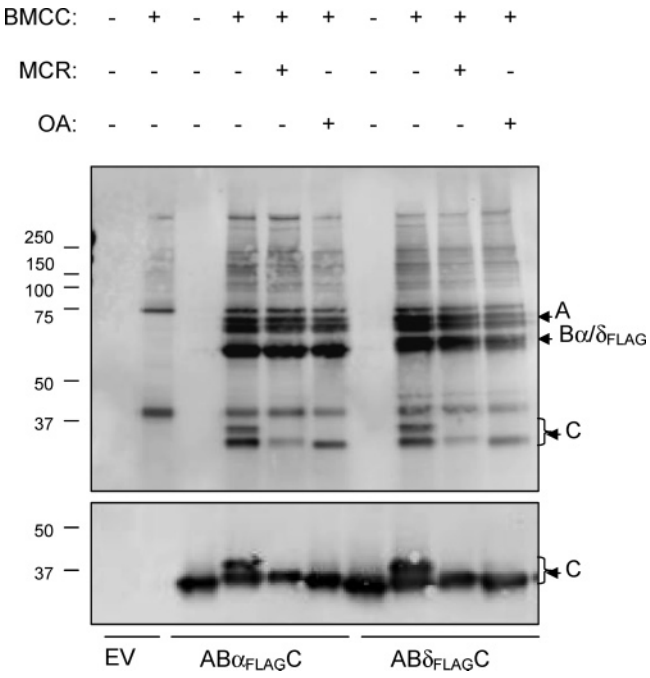

FIGURE 5: Phosphatase inhibitor pretreatment blocks adduction of PP2A subunits by BMCC. Equal amounts of FLAG peptide eluates of immunoprecipitation from cells expressing empty vector (EV), $B\alpha_{FLAG}$, or $B\delta_{FLAG}$ were incubated with 1 μM microcystin (MCR) or 1 μM okadaic acid (OA) for 30 min at 37 °C followed by a second incubation with 25 μM BMCC for 30 min at 37 °C. The adduct formation reaction was quenched by adding DTT, and the reaction mixtures were characterized by Western blotting with a mouse anti-biotin monoclonal antibody (top panel) and an antibody recognizing C subunit (bottom panel).

Competition Analysis. Because BMCC shows a distinct pattern of adduction on the PP2A catalytic subunit as compared to the adduction patterns of the A and B subunits, we examined the effect on BMCC adduction produced by two phosphatase inhibitors, microcystin-LR and okadaic acid. Both inhibitors interact with the PP2A catalytic subunit (*23*). The goal of these studies was to determine whether the electrophiles and phosphatase inhibitors share any common binding sites. BMCC adduction was completely blocked by microcystin-LR pretreatment and partially blocked by okadiac acid pretreatment as shown by Western blot analysis (Figure 5). Further analysis by LC-MS-MS showed that no Cys residues were adducted by BMCC after pretreatment with either inhibitor. This surprising result can be explained in part by the fact that microcystin binding overlaps with sites that are modified by BMCC (*23*). However, complete inhibition of BMCC adduction suggests that microcystin binding produces a conformational change sufficient to block access of BMCC to catalytic subunit cysteines.

DISCUSSION

In this study, we identified PP2A holoenzymes as targets of alkylation by model thiol-reactive electrophiles in vivo and in vitro. We mapped sites of modification by both electrophiles using LC-MS-MS and determined that site-specific adduction inhibits enzymatic activity. Selective alkylation of specific catalytic subunit cysteines is essential to enzyme inhibition. The susceptibility of these important regulatory enzymes to selective damage by electrophiles has important implications for toxicity and disease mechanisms that involve reactive intermediates.

To evaluate the effects of covalent adduction on enzymatic activity, we used purified FLAG-tagged PP2A holoenzymes treated with two biotinylated, thiol-reactive electrophiles, PEO-IAB and BMCC. The iodoacetamido moiety in PEO-IAB reacts with thiols by an S_N2 mechanism involving displacement of the iodide leaving group by the thiol, which mimics nucleophilic displacement reactions of aliphatic epoxides, episulfonium ions, and alkyl halides (*24*). The maleimido moiety of BMCC is a typical Michael acceptor, which reacts with thiols via 1,4-addition to its α,β-unsaturated carbonyl system (*24*). The chemistry is common in quinones, in many xenobiotic metabolites, and in many endogenous electrophiles generated by lipid and DNA oxidation (*25*). Thus, the chemistries of these probes mimic important thiol-reactive electrophiles generated in chemical toxicity and in inflammatory diseases. These probes penetrate cells, bind to diverse proteins, and elicit specific effects. Importantly, the biotin tag allows selective enrichment of probe-adducted proteins for subsequent analysis. We have recently demonstrated that PEO-IAB and BMCC selectively, yet reproducibly, modify over 500 proteins in subcellular fractions in vitro (*12*). Analysis of the sites of adduction revealed only approximately a 20% overlap in BMCC and PEO-IAB targets. The PEO-IAB congener IAB also exhibits selectivity in activating specific cellular stress responses. IAB, but not BMCC, activates electrophile stress via the transcription factor Nrf2; the difference between these probes can be attributed to selective adduction patterns on the sensor protein Keap1 (*11*). IAB and BMCC also exhibit differences in induction of ER stress and apoptosis in HEK 293 cells.[2]

In our previous work (*11*, *12*, *26*), LC-MS-MS proved to be a very sensitive and specific technique for the identification of individual residues as sites of chemical modification on proteins. Here we used LC-MS-MS to detect and identify the exact cysteine residues of PP2A that are modified by covalent adduction with thiol-reactive electrophiles, thus resulting in inhibition of enzymatic activity. Two isoforms of the PP2A holoenzymes, $AB\alpha_{FLAG}C$ and $AB\delta_{FLAG}C$, were treated in vitro with BMCC and PEO-IAB. The two compounds displayed strikingly different specificities for alkylation of the PP2A catalytic subunit in vitro, and only BMCC produced a significant decrease in enzymatic activity. PEO-IAB alkylated $PP2A_C$ only at Cys 266 and Cys 269, both of which are part of the loop domain between β12 and β13 that has been suggested as being critical for the inhibition of PP2A activity by the inhibitors microcystin-LR (*23*) and okadaic acid (*27*, *28*). In contrast, BMCC modified six cysteine residues, Cys 20, Cys 133, Cys 196, Cys 251, Cys 266, and Cys 269, which include the two sites adducted by PEO-IAB. These results are in agreement with previous studies, which revealed that maleimides are the most potent of several thiol-reactive electrophiles as inactivators of both PP1 and PP2A enzymes (*10*).

We used two different phosphatase activity assays, one employing the protein substrate histone H1 and the other using the small fluorogenic substrate DiFMUP, to show that the adduction of PEO-IAB to PP2A subunits has no effect

[2] N. Y. Shin, H. L. Wong, and D. C. Liebler, unpublished results.

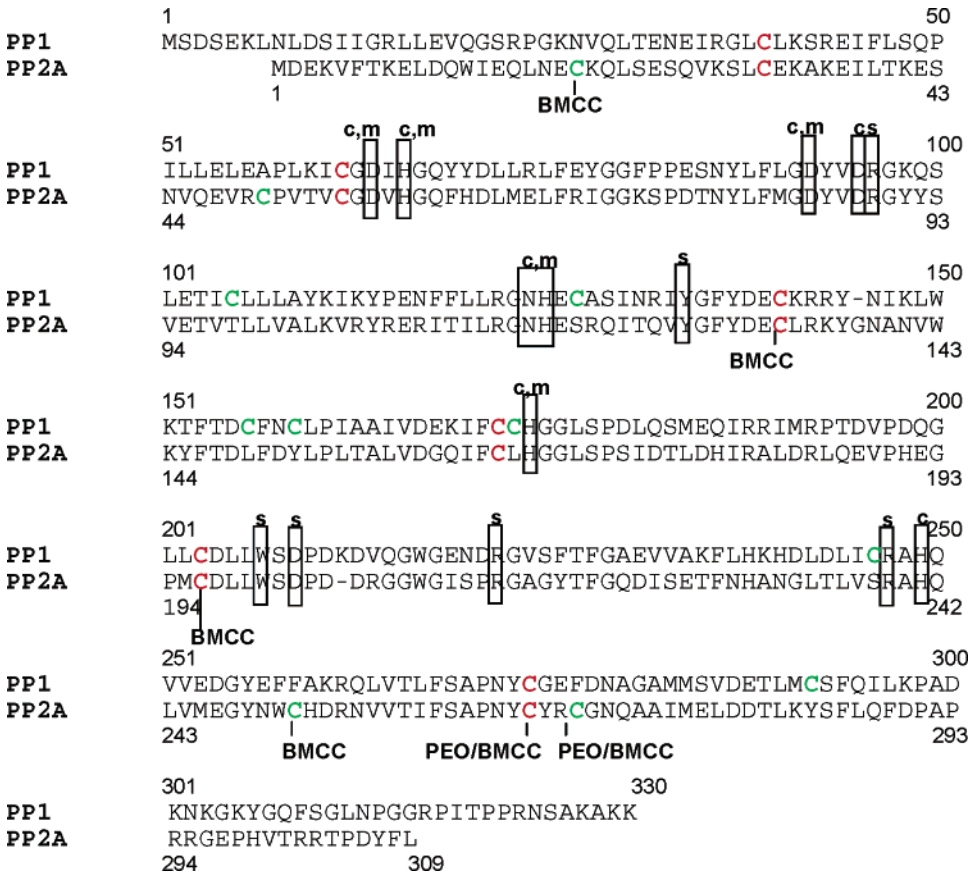

FIGURE 6: Sequence alignment of PP1 and PP2A catalytic subunits, α isoforms. Comparison of the two sequences indicates that the conserved part of the catalytic domain starts at residue 30 of PP1 and continues through residue 295. Six (red) out of 10 (green) Cys residues present in PP2A have a direct correspondent Cys residue with the PP1 amino acid sequence. Every active site residue of PP1 involved in substrate binding (s), metal coordination (m), or catalysis (c) is strictly conserved between the two enzymes so that the fold of the catalytic domain is expected to be closely preserved.

on enzymatic activity. Higher concentrations of PEO-IAB (up to 500 μM) can modify some adduct sites, yet only produced a very low (~20%) decrease in activity (Figure S2, Supporting Information). On the other hand, BMCC labeled three PP2A subunits and significantly decreased enzyme activity at much lower concentrations. Previous studies of the PP1 enzyme showed that the toxin microcystin-LR covalently adducted Cys 273 in the loop that connects β12 and β13 (corresponding to Cys 266 in PP2A) by a Michael-type addition (*29*). Both mutagenesis (*30*) and chemical modification (*31*) of Cys 273 failed to prevent inhibition by microcystin-LR. Thus, covalent adduction of microcystin-LR is not essential for the inhibition of the enzyme by the toxin. Other studies showed that Cys 269 in PP2A, which is also part of the loop formed between β12 and β13, plays an important role in inhibitor binding. Accordingly, okadaic acid binds to PP2A about 100 times more tightly than to PP1, which does not have a corresponding cysteine residue at that position (*28*) (Figure S10, Supporting Information). However, since both PEO-IAB and BMCC bind at these two sites and only BMCC decreases activity, we concluded that Cys 266 and Cys 269 are not essential sites for catalysis. Binding of an electrophile at these positions might weaken substrate binding to the active site by disturbing the structural relationship between the β12−β13 loop and the active sites, which may not be essential for enzymatic activity. This rationale suggests that modifications on PP2A most likely to affect catalysis occur on the four cysteine residues that bind BMCC only: Cys 20, Cys 133, Cys 196, and Cys 251. Of these, Cys 20 and Cys 251 are located close to the N-terminus and C-terminus, respectively, and far from the active site of the enzyme. These sites do not have a corresponding Cys residue in the PP1 sequence and, based on previous studies (*32*), do not appear to be directly involved in either substrate binding or catalysis. Thus, Cys 133 and Cys 196 represent the most likely sites for electrophile-induced inhibition of PP2A activity.

The catalytic subunit of PP2A holoenzyme contains six conserved cysteine residues, two of which were adducted by BMCC only (Cys 133 and Cys 196). While these residues are not thought to participate directly in catalysis, our observation that PP2A enzymatic activity is inhibited by thiol-reactive electrophiles indicates that modification of one or both of these cysteine residues of the catalytic subunit is sufficient to inhibit enzyme activity. A previous study of the kinetics of the inhibition of PP1 and PP2A by disulfides suggested that there is at least one residue whose integrity is essential for the enzymatic activity of both enzymes during the reaction; however, the identity of this residue(s) was not established (*10*). In this context, we suggest that one or both of the two cysteine residues of the PP2A holoenzyme that were modified *only* by BMCC and have a direct correspondent in the PP1 sequence are most likely responsible for the decrease in enzymatic activity when adducted. Careful analyses of the BMCC cysteine adduct maps for the two PP2A holoenzymes, ABα_{FLAG}C and ABδ_{FLAG}C, revealed that

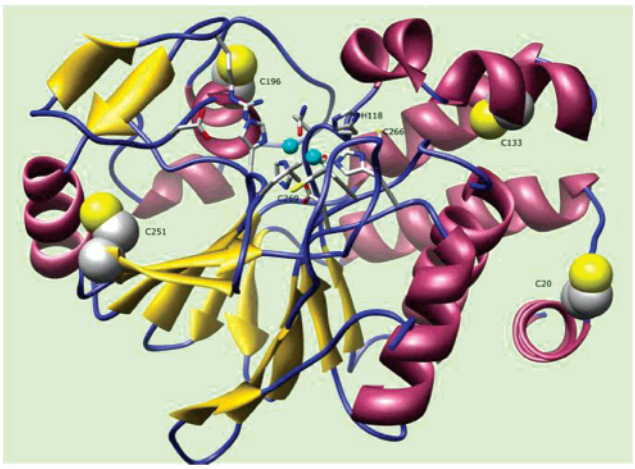

FIGURE 7: 3D view of a model of the catalytic subunit of PP2A generated with the software package Modeller using the structure of unlabeled PP1c (1S70) as a template. Cys residues adducted by BMCC only are shown as space-filling models (C20, C133, C196, C251) while the two Cys residues adducted by both PEO-IAB and BMCC are shown as sticks (C266, C269). The N-terminal subdomain binds the two metal ions (cyan) by several ligands highlighted as sticks. The figure was rendered with the program Chimera (*12*).

Cys 133 in the catalytic subunit is modified by BMCC on both, whereas Cys 196 is only modified in the Bδ-containing holoenzyme. Although these results suggest that Cys 133 is the sulfhydryl group whose modification by reactive electrophilic species leads to inactivation of PP2A, they do not exclude a role for Cys 196 adduction.

On the basis of the sequence alignment between PP1 and PP2A catalytic subunits, we observed that every active site residue of PP1 involved in metal coordination, substrate binding, or catalysis is strictly conserved in PP2A (Figure 6). Moreover, the hydrophobic or hydrophilic nature of the buried side chains in PP1 is conserved at virtually every position in PP2A, which further suggests that tertiary and quaternary structures of the two enzymes are very similar (*29*). Based on homology between the catalytic subunits of PP1 and PP2A, an initial model structure was generated for PP2A using EsyPred3D, a new automated homology modeling webserver (*20*). In this model, the spatial orientations of key active site residues are preserved with the only change in this region being the substitution of Leu 243 in PP2A for valine in PP1 (Figures 6 and 7). Structural superimposition of the initial PP2A model with that for microcystin-adducted PP1 (PDB ID 1FJM) revealed that the only major backbone structural difference was the conformation of the $\beta12-\beta13$ loop (Figure S11, Supporting Information). We speculate that this difference might mimic a physically plausible conformational change in protein conformation upon BMCC and PEO-IAB binding at the Cys 266 and Cys 269 positions. However, differences in reaction chemistries of the two compounds might stabilize different adduct orientations in different loop conformations with some affecting the enzymatic activity by decreasing substrate binding in the active site (for BMCC). Other adducts may be oriented away from the enzyme active site.

Further analysis of the model structure indicates that Cys 196 is located at a distance of 12.2 Å (Cβ to Cγ distance) away from Asp 202, an active site residue conserved in all protein phosphatases that likely helps to maintain the conformation of Arg 214 via a hydrogen bond with its ϵ nitrogen (Figure 8, upper panel) (*33*). Arg 214 was predicted to contribute to phosphosubstrate binding as well as to stabilize the pentacoordinate transition state (*33*). Covalent adduction with a BMCC molecule (~33 Å long) at Cys 196 could decrease enzymatic activity by disrupting the substrate binding mode in the active site due to steric effects on important residues in this region of the enzyme (Figure 8). Cys 133 is located at a distance of 12.0 Å from His 118, a residue predicted to be directly involved in catalysis (*29*). A covalent adduction with a BMCC molecule (~33 Å long) at Cys 133 could potentially perturb the orientation of the His 118 catalytic residue toward the phosphosubstrate and thereby decrease enzymatic activity.

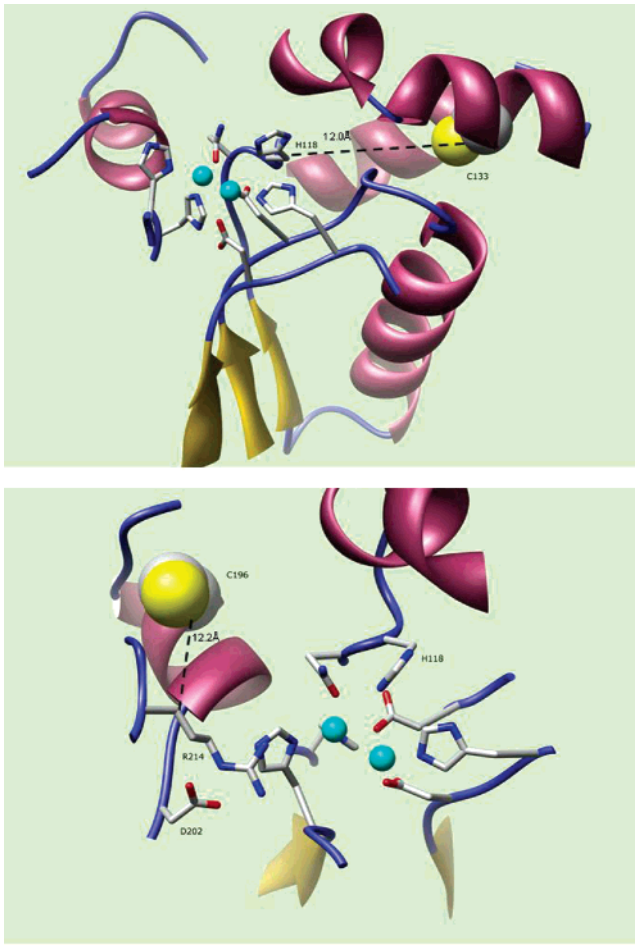

FIGURE 8: Enlarged 3D view of a model of the catalytic subunit of PP2A. The top structure shows the C196 that is 12.2 Å from D202, an active site residue conserved in all protein serine/threonine phosphatases, which is likely to help to maintain the conformation of R214 via a salt bridge (*12*). R214 was predicted to contribute to phosphosubstrate binding. The bottom structure shows the C133 that is 12.0 Å from H118, the residue predicted to be involved in catalysis (*12*). The figures were rendered with the program Chimera (*12*).

These studies build on previous work describing the ability of alkylating electrophiles to inhibit protein phosphatases (*10*). Here we have applied model electrophile probes that exhibit chemistries relevant to diverse biological reactive intermediates. The data indicate the importance of selective modification in determining the outcome of covalent adduction reactions involved in protein damage. The two probes studied represent generic thiol-reactive electrophile chemistries, yet the structures of the probes and the chemistry of

the electrophiles translated to functionally important differences in the sites and consequences of adduction. The identification of specific sites linked to PP2A inactivation suggests that specific assays for adducted forms of these sequences could provide a general means of screening PP2A inhibitors. Evaluation of the utility of such an approach is currently underway in our laboratories.

ACKNOWLEDGMENT

We thank Prof. Terry Lybrand and Prof. Jens Meiler for helpful discussions and comments on the manuscript.

SUPPORTING INFORMATION AVAILABLE

One table of the sites of BMCC and PEO-IAB modification for the A and Bα/δ subunits of the PP2A holoenzyme, the MS-MS spectra for all six BMCC-adducted peptides and the two PEO-IAB-adducted peptides of the catalytic subunit of PP2A holoenzyme, the sequence alignment of the catalytic subunit of the PP1 δ isoform (used as a template for modeling) and the catalytic subunit of PP2A α isoform, and an additional 3D view of the model of the catalytic subunit of the PP2A α isoform. This material is available free of charge via the Internet at http://pubs.acs.org.

REFERENCES

1. Stone, R. L., and Dixon, J. E. (1994) Protein-tyrosine phosphatases, *J. Biol. Chem. 269*, 31323−31326.
2. Barford, D., Das, A. K., and Egloff, M. P. (1998) The structure and mechanism of protein phosphatases: insights into catalysis and regulation, *Annu. Rev. Biophys. Biomol. Struct. 27*, 133−164.
3. Rhee, S. G., Bae, Y. S., Lee, S. R., and Kwon, J. (2000) Hydrogen peroxide: a key messenger that modulates protein phosphorylation through cysteine oxidation, *Sci. STKE 2000*, E1.
4. Foley, T. D., and Kintner, M. E. (2005) Brain PP2A is modified by thiol-disulfide exchange and intermolecular disulfide formation, *Biochem. Biophys. Res. Commun. 330*, 1224−1229.
5. Liebler, D. C., and Guengerich, F. P. (2005) Elucidating mechanisms of drug-induced toxicity, *Nat. Rev. Drug Discov. 4*, 410−420.
6. West, J. D., and Marnett, L. J. (2006) Endogenous reactive intermediates as modulators of cell signaling and cell death, *Chem. Res. Toxicol. 19*, 173−194.
7. Dinkova-Kostova, A. T., Holtzclaw, W. D., and Kensler, T. W. (2005) The role of Keap1 in cellular protective responses, *Chem. Res. Toxicol. 18*, 1779−1791.
8. Janssens, V., and Goris, J. (2001) Protein phosphatase 2A: a highly regulated family of serine/threonine phosphatases implicated in cell growth and signalling, *Biochem. J. 353*, 417−439.
9. Zolnierowicz, S. (2000) Type 2A protein phosphatase, the complex regulator of numerous signaling pathways, *Biochem. Pharmacol. 60*, 1225−1235.
10. Nemani, R., and Lee, E. Y. (1993) Reactivity of sulfhydryl groups of the catalytic subunits of rabbit skeletal muscle protein phosphatases 1 and 2A, *Arch. Biochem. Biophys. 300*, 24−29.
11. Hong, F., Sekhar, K. R., Freeman, M. L., and Liebler, D. C. (2005) Specific patterns of electrophile adduction trigger Keap1 ubiquitination and Nrf2 activation, *J. Biol. Chem. 280*, 31768−31775.
12. Dennehy, M. K., Richards, K. A. M., Wernke, G. W., Shyr, Y., and Liebler, D. C. (2006) Cytosolic and nuclear protein targets of thiol-reactive electrophiles, *Chem. Res. Toxicol. 9*, 20−29.
13. Strack, S., Chang, D., Zaucha, J. A., Colbran, R. J., and Wadzinski, B. E. (1999) Cloning and characterization of B delta, a novel regulatory subunit of protein phosphatase 2A, *FEBS Lett. 460*, 462−466.
14. Adams, D. G., Coffee, R. L., Jr., Zhang, H., Pelech, S., Strack, S., and Wadzinski, B. E. (2005) Positive regulation of Raf1-MEK1/2-ERK1/2 signaling by protein serine/threonine phosphatase 2A holoenzymes, *J. Biol. Chem. 280*, 42644−42654.
15. Jakes, S., and Schlender, K. K. (1988) Histone H1 phosphorylated by protein kinase C is a selective substrate for the assay of protein phosphatase 2A in the presence of phosphatase 1, *Biochim. Biophys. Acta 967*, 11−16.
16. Strack, S., Westphal, R. S., Colbran, R. J., Ebner, F. F., and Wadzinski, B. E. (1997) Protein serine/threonine phosphatase 1 and 2A associate with and dephosphorylate neurofilaments, *Brain Res. Mol. Brain Res. 49*, 15−28.
17. Ham, A. J. (2005) Proteolytic Digestion Protocols, in *The Encyclopedia of Mass Spectrometry*, Vol. 2, Biological Applications, Part A, Peptides and Proteins (Caprioli, R. M., and Gross, M. L., Eds.) pp 10−17, Elsevier, Kidlington, Oxford, U.K.
18. Yates, J. R., Eng, J. K., McCormack, A. L., and Schieltz, D. (1995) Method to correlate tandem mass spectra of modified peptides to amino acid sequences in the protein database, *Anal. Chem. 67*, 1426−1436.
19. Hansen, B. T., Davey, S. W., Ham, A. J., and Liebler, D. C. (2005) P-Mod: An algorithm and software to map modifications to peptide sequences using tandem MS data, *J. Proteome Res. 4*, 358−368.
20. Lambert, C., Leonard, N., De, B. X., and Depiereux, E. (2002) ESyPred3D: Prediction of proteins 3D structures, *Bioinformatics 18*, 1250−1256.
21. Pettersen, E. F., Goddard, T. D., Huang, C. C., Couch, G. S., Greenblatt, D. M., Meng, E. C., and Ferrin, T. E. (2004) UCSF Chimera—a visualization system for exploratory research and analysis, *J. Comput. Chem. 25*, 1605−1612.
22. Groves, M. R., Hanlon, N., Turowski, P., Hemmings, B. A., and Barford, D. (1999) The structure of the protein phosphatase 2A PR65/A subunit reveals the conformation of its 15 tandemly repeated HEAT motifs, *Cell 96*, 99−110.
23. Honkanen, R. E., Zwiller, J., Moore, R. E., Daily, S. L., Khatra, B. S., Dukelow, M., and Boynton, A. L. (1990) Characterization of microcystin-LR, a potent inhibitor of type 1 and type 2A protein phosphatases, *J. Biol. Chem. 265*, 19401−19404.
24. Guengerich, F. P., and Liebler, D. C. (1985) Enzymatic activation of chemicals to toxic metabolites, *Crit. Rev. Toxicol. 14*, 259−307.
25. Marnett, L. J., Riggins, J. N., and West, J. D. (2003) Endogenous generation of reactive oxidants and electrophiles and their reactions with DNA and protein, *J. Clin. Invest. 111*, 583−593.
26. Hong, F., Freeman, M. L., and Liebler, D. C. (2005) Identification of sensor cysteines in human Keap1 modified by the cancer chemopreventive agent sulforaphane, *Chem. Res. Toxicol. 18*, 1917−1926.
27. Evans, D. R., and Simon, J. A. (2001) The predicted beta12-beta13 loop is important for inhibition of PP2Acalpha by the antitumor drug fostriecin, *FEBS Lett. 498*, 110−115.
28. Zhang, Z., Zhao, S., Long, F., Zhang, L., Bai, G., Shima, H., Nagao, M., and Lee, E. Y. (1994) A mutant of protein phosphatase-1 that exhibits altered toxin sensitivity, *J. Biol. Chem. 269*, 16997−17000.
29. Goldberg, J., Huang, H. B., Kwon, Y. G., Greengard, P., Nairn, A. C., and Kuriyan, J. (1995) Three-dimensional structure of the catalytic subunit of protein serine/threonine phosphatase-1, *Nature 376*, 745−753.
30. Zhang, Z., Zhao, S., ans-Zirattu, S., Bai, G., and Lee, E. Y. (1993) Mutagenesis of the catalytic subunit of rabbit muscle protein phosphatase-1, *Mol. Cell. Biochem. 127−128*, 113−119.
31. Moorhead, G., MacKintosh, R. W., Morrice, N., Gallagher, T., and MacKintosh, C. (1994) Purification of type 1 protein (serine/threonine) phosphatases by microcystin-Sepharose affinity chromatography, *FEBS Lett. 356*, 46−50.
32. Teruya, T., Simizu, S., Kanoh, N., and Osada, H. (2005) Phoslactomycin targets cysteine-269 of the protein phosphatase 2A catalytic subunit in cells, *FEBS Lett. 579*, 2463−2468.
33. Huang, H. B., Horiuchi, A., Goldberg, J., Greengard, P., and Nairn, A. C. (1997) Site-directed mutagenesis of amino acid residues of protein phosphatase 1 involved in catalysis and inhibitor binding, *Proc. Natl. Acad. Sci. U.S.A. 94*, 3530−3535.

BI060551N